applied sciences

MDPI

Article

Generation and Measurement of Squeezed Vacuum States at Audio-Band Frequencies

Yinghao Gao [1], Jinxia Feng [1,2,*], Yuanji Li [1,2] and Kuanshou Zhang [1,2]

[1] State Key Laboratory of Quantum Optics and Quantum Optics Devices, Institute of Opto-Electronics, Shanxi University, Taiyuan 030006, China; 18835127113@163.com (Y.G.); fengjx@sxu.edu.cn (Y.L.); liyuanji@sxu.edu.cn (K.Z.)

[2] Collaborative Innovation Center of Extreme Optics, Shanxi University, Taiyuan 030006, China

* Correspondence: fengjx@sxu.edu.cn

Received: 30 January 2019; Accepted: 21 March 2019; Published: 27 March 2019

Abstract: Squeezed vacuum states at audio-band frequencies are important quantum resources for practical applications. We demonstrated the generation of squeezed vacuum states at the audio-band frequencies from a subthreshold optical parametric oscillator with a periodically poled $KTiOPO_4$ crystal pumped by a homemade continuous wave single-frequency dual-wavelength laser. To detect squeezed vacuum states at audio-band frequencies, the influences of the local oscillator (LO) power, the common mode rejection ratio (CMRR) of balanced homodyne detectors, and the phase jitter between the LO and squeezed vacuum field on the measurement of squeezed vacuum states at audio-band frequencies were considered. By optimizing the LO power, improving the CMRR of photodetectors to 67 dB based on the design of differential fine-tuning circuit and adjustable bias voltage, and reducing the phase jitter between the LO and squeezed vacuum field to 1.7° with the help of the coherent locking technique, 6.1 ± 0.3 dB squeezed vacuum states at audio frequencies from 5 kHz to 20 kHz were generated. A 3.0 ± 0.3 dB phase squeezed vacuum state was obtained at the audio frequency of 3.5 kHz.

Keywords: squeezed vacuum states; audio-band frequencies; subthreshold optical parametric oscillator

1. Introduction

Squeezed vacuum states at audio-band frequencies are potentially useful for gravitational wave detection [1,2], quantum storage and communication [3–5], all-atomic magnetometer [6,7], and biological measurement [8]. In these application fields, since the quantum noise can be reduced by injecting squeezed vacuum states, the sensitivity or signal-to-noise ratio for measurements at audio-band frequencies can be improved. Besides four-wave-mixing technique being demonstrated to generate intensity difference squeezing at audio-band frequencies [9], most squeezed vacuum states at audio-band frequencies are generated using a subthreshold optical parametric oscillator (OPO) [10–13]. Thus far, a maximum squeezing of 11.6 dB at audio-band frequencies is reported in Ref [13].

A balanced homodyne detector (BHD) is a perfect device for the detection of squeezed vacuum states [14]. For squeezed vacuum states, the variance of a certain field quadrature is found to be squeezed below the variance of the corresponding vacuum field. Since the laser noise reaches the shot noise level (SNL) at MHz range, it is easy to measure and obtain squeezed vacuum states at high frequency range by using the BHD system. Compared with the observation of squeezing spectrum at high frequency range, the observation of that at audio-band frequencies is relatively difficult, as the intensity noise of the local oscillator (LO) for the BHD system is far beyond the SNL and actual detectors in the BHD cannot eliminate the classical noise of the LO thoroughly. The measured squeezing vacuum

level at audio-band frequencies can be improved by suppressing the low frequency classical noise of the laser [15], reducing the phase jitter between the LO and squeezed vacuum fields [16] and increasing the level of the common mode rejection ratio (CMRR) of detectors in the BHD [17].

In this study, squeezed vacuum states at audio-band frequencies were generated from a subthreshold OPO with a periodically poled $KTiOPO_4$ (PPKTP) crystal pumped by a homemade continuous wave (cw) single-frequency dual-wavelength laser. The influences of the LO power, the CMRR of detectors in the BHD, and the phase jitter between the LO and squeezed vacuum fields were considered in the measurement of squeezed vacuum states at audio-band frequencies. To improve the measured squeezing vacuum level at audio-band frequencies, the power of LO for the BHD system was optimized; the CMRR of the BHD at audio-band frequencies was improved by the design of differential fine-tuning circuit and adjustable bias voltage; and the phase jitter between the LO and squeezed vacuum fields was reduced using the coherent locking scheme.

2. Theoretical Analysis

Squeezed vacuum states can be obtained when the OPO is operated below the threshold. The variance of the generated squeezed $V_s^-(\Omega)$ and anti-squeezed $V_s^+(\Omega)$ quadrature can be expressed by [16]

$$V_s^{\pm}(\Omega) = 1 \pm 4\eta_{esc}\eta_{\mathrm{det}}\eta_{prop}\eta_{\mathrm{hom}} \times \frac{\sqrt{P/P_{\mathrm{th}}}}{\left(1 \mp \sqrt{P/P_{\mathrm{th}}}\right)^2 + 4\Omega^2}, \quad (1)$$

where $\eta_{esc} = T/(T + L)$ is the cavity escape efficiency, T is the transmittance of output coupler, L is the intracavity losses, η_{det} is the quantum efficiency of the photodetector, η_{prop} is the propagation efficiency, $\eta_{\mathrm{hom}} = V^2$ is the homodyne detection efficiency [18], V is the fringe visibility for the LO and a bright alignment beam in the BHD system, P is the pump power of the OPO, P_{th} is the threshold of the OPO, $\Omega = 2\pi f/\gamma$ is normalized frequency, f is the analysis frequency, $\gamma = c(T + L)/l$ is the OPO cavity decay rate, c is the speed of light in the vacuum and l is round trip length of the cavity.

The noise power of squeezed vacuum states can be detected by the BHD system. The measured field ($\hat{a} = \alpha + \delta\hat{a}$) and LO ($\hat{b} = \beta + \delta\hat{b}$) are combined at a 50/50 beam splitter and detected by a pair of photodetectors with quantum efficiency of η_{det1} and η_{det2}, respectively. $\delta\hat{a}$ and $\delta\hat{b}$ are fluctuations around the mean field values of the measured field (α) and LO (β), respectively. Assuming the mean field of the measured field α is far smaller than β, the items related to the mean field of the measured field can be ignored, and the photocurrent subtraction from the two photodetectors can be written by [19]

$$I = \frac{\eta_{\mathrm{det1}}}{2}\left(\beta\delta\hat{X}_a(\theta) + \beta\delta\hat{X}_{LO}(\theta)\right) + \frac{\eta_{\mathrm{det1}}}{2}\beta^2 - \frac{\eta_{\mathrm{det2}}}{2}\left(-\beta\delta\hat{X}_a(\theta) + \beta\delta\hat{X}_{LO}(\theta)\right) - \frac{\eta_{\mathrm{det2}}}{2}\beta^2, \quad (2)$$

where $\delta\hat{X}_{LO}(\theta)$ is the quadrature fluctuation operator for the LO at relative phase (θ) between the LO and measured field. $\delta\hat{X}_a(\theta)$ is the quadrature fluctuation operator for the measured field.

Because the intensity noise of the LO is far beyond the SNL at audio-band frequencies, the measured squeezing level of the squeezed vacuum states at audio-band frequencies is related to not only the losses above-mentioned in Equation (1), but also the intensity noise of the LO and the CMRR of photodetectors in the BHD. To improve the CMRR, a single electronic board design is usually employed to reduce the influence from the discrepancy of electronics components, where the photocurrents of both photodiodes are directly subtracted before any further electronic signal processing [20]. However, the discrepancy from parameters of both photodiodes, including their quantum efficiencies, equivalent capacitances, equivalent resistances, etc., is also a crucial factor to decrease the CMRR of photodetectors. If we define an unbalanced factor related to the CMRR of photodetectors, i.e. $G = \sigma\eta_{\mathrm{det2}}/\eta_{\mathrm{det1}}$, the variances of the photocurrent subtraction can be written as [19]

$$V(I) = \frac{\beta^2\eta_{\mathrm{det1}}^2}{4}\left((1 + G)^2V_a + (1 - G)^2V_{LO}\right), \quad (3)$$

where σ represents the unbalanced item induced from the discrepancy of electronics components, V_{LO} is the intensity noise of the LO, and V_a is the variances of the measured field. $V_a = V_s^-(\Omega)$ when the measured field is the generated squeezed vacuum state.

Considering the intensity noise of the LO and the CMRR of photodetectors, the measured value of squeezing level can be expressed by

$$V_s' = \frac{V_s^-(\Omega)(1+G)^2 + V_{LO}(1-G)^2}{(1+G)^2 + V_{LO}(1-G)^2}, \tag{4}$$

According to the definition of CMRR, the value of the CMRR can be expressed as [19]

$$R_{CMRR} = 10\lg\frac{P_{com}}{\Delta \times P_{com}} = 20\lg\frac{1+G}{2|1-G|}, \tag{5}$$

where P_{com} is the measured power from one photodetector when the other one is blocked, and $\Delta \times P_{com}$ is the measured power when both photodetectors are illuminated. G can be given as [19]

$$G = \frac{2 \times 10^{R_{CMRR}/20} - 1}{2 \times 10^{R_{CMRR}/20} + 1}, \tag{6}$$

Another influence issue on the measured squeezing level is the phase jitter effect. The relative phase between the LO and squeezed vacuum fields determines the measured quadrature of squeezed vacuum sates. The jitter of the phase relation caused by residual high frequency phase modulations will reduce the level of measured squeezing. Assuming that the relative phase between the LO and squeezed vacuum field has a normal distribution with a jitter of $\delta\varphi$, the measured squeezing level can be written by [16]

$$V_s^-(\Omega)\big|_{\delta\varphi} = V_s^+(\Omega)\cos^2\delta\varphi + V_s^-(\Omega)\sin^2\delta\varphi, \tag{7}$$

Figure 1 shows the theoretical calculated normalized noise power of squeezed vacuum states at the analysis frequency of 5 kHz with respect to different values of V_{LO}, R_{CMRR} and $\delta\varphi$ considering an actual squeezed vacuum states generation and measurement system with the experimental parameters of η_{esc} = 0.95, η_{det} = 0.96, η_{prop} = 0.94, η_{hom} = 0.98, P = 100 mW, P_{th} = 350 mW, T = 0.13, L = 0.012, and l = 33 mm. Solid Curve (i), which is calculated by Equation (1), is the squeezing level without considering the influence of the unbalance factor G and the intensity noise of the LO. It can be seen that the theoretical calculated squeezing level is 6.25 dB that is not dependent on the CMRR of the detectors. Solid Curves (ii)–(iv) are the theoretical calculated squeezing levels using Equation (2) with the same experimental parameters and considering the influence of the unbalance factor G and V_{LO} exceeding the SNL 0 dB, 35 dB and 50 dB, respectively. According to Curve (ii), the value of the squeezing level is still influenced by the CMRR of the detectors when its value is less than 20 dB, even if the intensity noise of the LO reaches the SNL. From Curves (iii) and (iv), it can be seen that the critical values of the CMRR of the detectors, at which the squeezing level will not be influenced by the intensity noise of the LO, are 54 dB and 70 dB when the intensity noise of the LO is 35 dB and 50 dB above the SNL, respectively. Dashed Curves (a)–(d) are the theoretical calculated squeezing levels using Equation (2) except that the variance of the generated squeezed $V_s^-(\Omega)|_{\delta\varphi}$ is substituted for $V_s^-(\Omega)$ in Equation (7) considering the influence of a phase jitter of $\delta\varphi = 2^\circ$ on the measured squeezing level. Two-degree phase jitter is a typical value in the common experimental setup used to generate squeezed vacuum states. According to dashed Curve (a), the theoretical calculated squeezing level is reduced from 6.25 dB to 6.05 dB caused by 2° phase jitter without considering the influence of the unbalance factor G and the intensity noise of the LO. Dashed Curves (b)–(d) are the theoretical calculated squeezing levels considering the influence of 2° phase jitter, the unbalance factor G and V_{LO} exceeding the SNL 0 dB, 35 dB and 50 dB, respectively. The phase jitter effect becomes an important issue with the increasing of squeezing level. Consequently, the measured squeezing level of squeezed vacuum states at audio-band

frequencies can be improved by suppressing the excess intensity noise of the LO, increasing the value of CMRR of detectors and reducing the phase jitter when the relative phase between the LO and squeezed vacuum fields is locked.

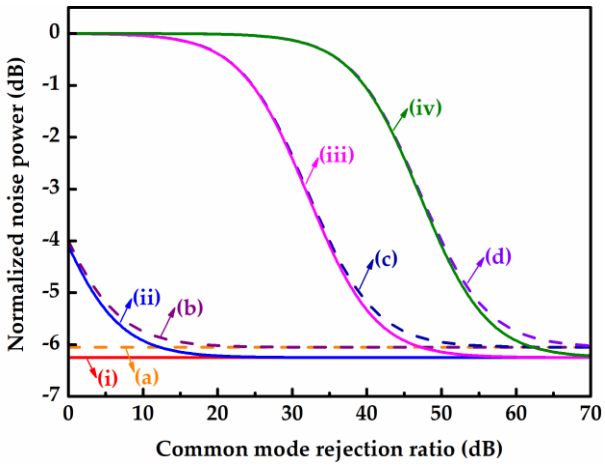

Figure 1. Dependence of normalized noise power of squeezed vacuum states at the analysis frequency of 5 kHz on the R_{CMRR}, the phase jitter and V_{LO}: Curves (i) and (a), $G = 1$, $V_{LO} = 0$ dB with $\delta\varphi = 0°$ and 2°, respectively; Curves (ii)–(iv) and (b)–(d), $G \neq 1$ and V_{LO} exceeds the SNL 0 dB, 35 dB and 50 dB with $\delta\varphi = 0°$ and 2°, respectively.

3. Experimental Setup

The schematic of the experimental setup used to generate squeezing vacuum states is shown in Figure 2. The laser source was a homemade low noise cw single-frequency dual-wavelength laser with output power of 7 watts at 532 nm and 3 watts at 1064 nm. Optical isolators (OIs) were used to eliminate the back-reflection light of the infrared and green laser. The longitudinal mode of the laser was monitored by a scanning Fabry-Perot (F-P1) interferometer. A small part of the infrared laser was injected into the F-P2, which was used as a frequency standard to lock the frequency of the laser. The frequency shift was less than $\pm$1.5 MHz for a given 1 h when the laser was frequency stabilized employing the Pound-Drever-Hall (PDH) technique [21].

The main part of the infrared laser and the green laser were sent through a ring mode cleaner (MC1) cavity with a finesse of 300 and a linewidth of 1.0 MHz and MC2 with a finesse of 270 and a linewidth of 1.1 MHz, respectively, for filtering the laser spatial mode and excess intensity noise. The two MCs were locked by the PDH technique. The power transmittances of the two MCs were approximately 78%. Using the MCs, the intensity noises of the infrared and green laser reached the SNL for analysis frequencies higher than 1.8 MHz. The infrared output from MC1 was divided into three parts and used as the LO beam for the BHD system, the auxiliary beam to lock the length of the subthreshold OPO cavity and the coherent control field (CCF) to control the relative phase between the LO and squeezed vacuum states, separately. The green output from MC2 acted as the pump of the OPO.

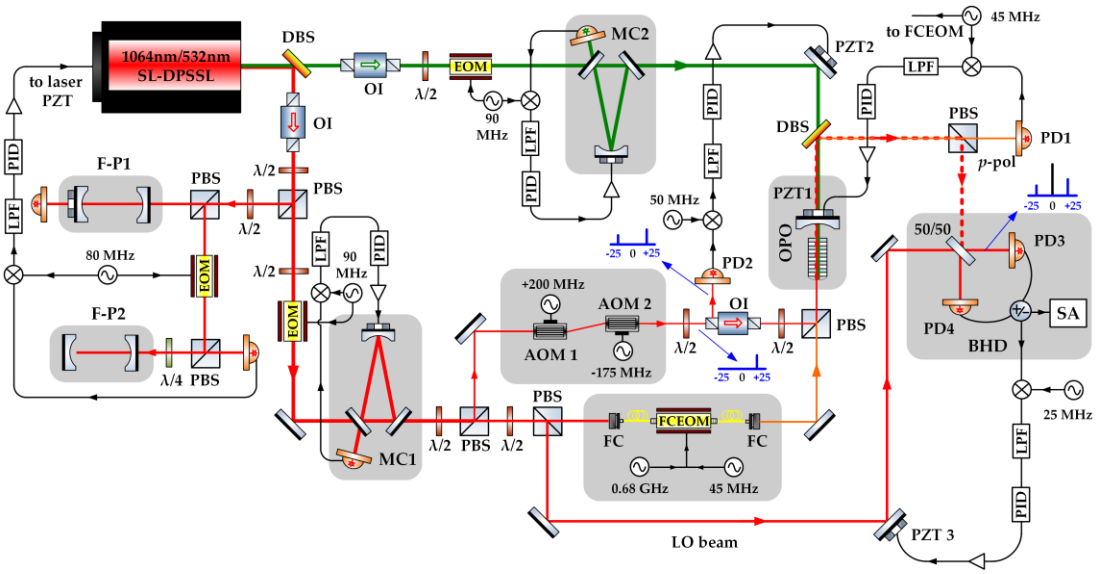

Figure 2. Schematic of the experimental setup used to generate squeezed vacuum states. OI, Optical isolator; F-P, Fabry–Perot cavity; MC, mode cleaner; FC, fiber coupler; EOM, electro-optical modulator; FCEOM, fiber coupled EOM; AOM, acousto-optic modulator; OPO, optical parametric oscillator; DBS, dichroic beam splitter; PBS, polarizing beam splitter; λ/2, half wave plate; λ/4, quarter wave plate; PZT, piezo-electric transducer; PD, photodetector; SA, spectrum analyzer; PID, proportional-integral-derivative; LPF, low pass filter; ◁, high voltage amplifier; ⊗, mixer; +/−, positive/negative power combiner; ⏲, signal generator.

The OPO was a semi-monolithic cavity composed of a PPKTP crystal with dimensions of 10 mm (length) × 2 mm (width) × 1 mm (thickness) and a concave mirror with a radius of 25 mm. The concave face of concave mirror acted as input and output couplers was partial transmission coated at 1064 nm and 532 nm ($T_{1064\,\mathrm{nm}}$ = 13% and $T_{532\,\mathrm{nm}}$ = 80%). The flat face of concave mirror was antireflection (AR) coated at 1064 nm and 532 nm ($R_{1064\text{ and }532\mathrm{nm}} < 0.2\%$). One end of the PPKTP crystal was convex surface with a radius of 12 mm and HR coated at 1064 nm and 532 nm ($R_{1064\text{ and }532\mathrm{nm}} > 99.9\%$). Another end of the PPKTP crystal was flat surface and AR coated at 1064 nm and 532 nm ($R_{1064\text{ and }532\mathrm{nm}} < 0.2\%$). The concave mirror was mounted on a piezo-electric transducer (PZT1) to control the length of OPO cavity. The PPKTP crystal was housed in a copper oven and temperature-controlled by a homemade temperature controller with an accuracy of 0.01 °C. The temperature of PPKTP was controlled at 40.0 °C to realize the optimum phase matching. The optical cavity length of the OPO was 33 mm and the measured linewidth was 102 MHz. PPKTP is a type-I phase matched crystal. The *s*-polarized squeezed vacuum states from the subthreshold OPO was generated when pump power of green laser was below the threshold of OPO, which was separated from the residual pump field by a dichroic beam splitter (DBS). The generated squeezed vacuum states were measured using the BHD system and recorded by a spectrum analyzer (SA).

The auxiliary beam was generated by frequency shifting 1064 nm laser using a fiber-coupled electro-optical modulator (FCEOM), which was driven by a sinusoidal signal. The *p*-polarized auxiliary beam was injected into the OPO cavity. When the modulated frequency of sinusoidal signal is 680 MHz, the auxiliary beam can be simultaneous resonant in the OPO with the *s*-polarized squeezed vacuum field. The transmission of auxiliary beam from the OPO was spatially separated with the squeezed vacuum field by a polarization beam splitter (PBS) and detected by a photodetector (PD1). The subthreshold OPO cavity was locked by PDH technique with a radio frequency of 45 MHz via the *p*-polarized auxiliary beam. The error signal was fed back to PZT1 to lock the subthreshold OPO cavity. Another portion of 1064 nm laser from MC1 passed through an acousto-optic modulator (AOM1) with a shifted frequency of 200 MHz and an AOM2 with a shifted frequency of −175 MHz, respectively. The output beam is used as the CCF with a frequency shift of Ω = 25 MHz. The CCF was injected

to the subthreshold OPO and the outgoing CCF from the subthreshold OPO was detected by PD2. After the photocurrent from PD2 was demodulated by a sinusoidal signal with frequency of 50 MHz and then filtered by a low-pass filter (LPF) with bandwidth of 1.9 MHz, the demodulated and filtered current was used as the error signal and fed back to the PZT2 to lock the relative phase between the pump field and CCF.

The noise power of down-conversion fields from the subthreshold OPO was measured by the BHD system. The down-conversion fields and LO were combined at a 50/50 beam splitter and detected by a pair of InGaAs photodiodes. By the way, the laser intensity noise of the LO was measured by the BHD when the pump and CCF were blocked. The sum of two photocurrents from PD3 and PD4 was the LO intensity noise using a positive power combiner, the subtraction of two photocurrents was the SNL using a negative power combiner. When the pump and CCF were injected, squeezed vacuum states were generated. The generated squeezed vacuum states were measured by the BHD and the alternating current (AC) part of photocurrent subtraction was recorded by the SA. Another AC part of photocurrent subtraction was demodulated by a radio frequency of 25 MHz, and then filtered by an LPF with bandwidth of 1.9 MHz. This demodulated and filtered current was used as the error signal and fed back to PZT3 to lock the relative phase between the CCF and LO, i.e., to lock the relative phase between the LO beam and the squeezed vacuum states. Thus, a stable measurement result can be achieved.

For improving the CMRR of two photodetectors, a self-subtraction photodetector scheme was firstly designed on a single electronic board to reduce the influence of the discrepancy of electronics components. The photocurrents of both photodiodes are directly subtracted before any further electronic signal processing, as shown in Figure 3a. Furthermore, an equivalent circuit of photodiode, as shown in Figure 3b, was designed to compensate for the asymmetry of the parameters of two photodiodes (PD1 and PD2), due to it is almost impossible to choose two photodiodes with identical parameters. The differential fine-tuning circuit between two photodiodes was built and the differential photocurrent was obtained by differential operation of two optical signals. The adjustable bias voltage (BV) was set on each photodiode, which were supplied by two stable sources with adjustable ranges of from 3 to 15 V and from −15 to −3 V, respectively. When the ratio of the equivalent capacitance of two photodiodes was adjusted, the difference from the equivalent capacitance was compensated effectively. Resistors R_1 and R_2 were fixed to compensate coarsely the series resistance, which made the resistance approximately same above and below joint Z. The series resistance above and below joint Z were strictly equal by finely tuning an adjustable resistor R_3. Consequently, the phase discrepancy of output current signal of both photodiodes induced by unequal equivalent resistance and capacitance was compensated. In comparison to the self-subtraction detector without the differential fine-tuning circuit and adjustable BV, the CMRR was strongly improved from the original 20 dB to 67 dB.

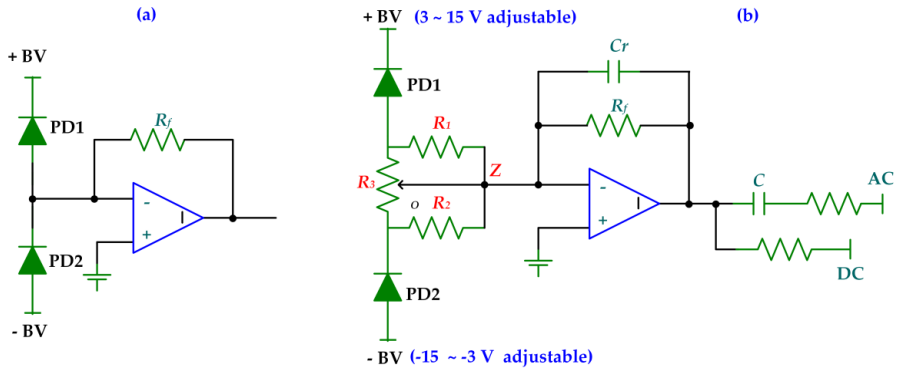

Figure 3. Schematic of the circuit of photodetector: (**a**) the self-subtraction photodetector scheme; and (**b**) the self-subtraction photodetector scheme with the differential fine-tuning circuit and adjustable BV.

4. Results

To optimize the power of the LO, when the pump and CCF was blocked, the intensity noise of the LO was measured by the BHD system firstly. The measured noise power of the LO at analysis frequencies from 2 kHz to 200 kHz was recorded by SA with a resolution bandwidth (RBW) of 51 Hz, a video bandwidth (VBW) of 110 Hz and the sweep time of 1 s. When the total power of the LO was 1 mW, that is, two photodiodes (FD500, Fermionics Opto-Technology) were illuminated by the power of 500 μW, respectively, the measured noise power of the LO is shown in Figure 4. Curve (i) is the SNL; Curve (ii) is the intensity noise of the LO; and Curve (iii) is the electronic noise level (ENL). The intensity noise of the LO was more than 25 dB above the SNL and the SNL was 18 dB above the ENL at analysis frequencies from 2 kHz to 200 kHz, respectively. At the audio frequency of 5 kHz, the intensity noise of the LO was 30 dB above the SNL. The intensity noise of the LO at analysis frequencies from 0.2 MHz to 5 MHz was recorded by SA with an RBW of 110 kHz, a VBW of 110 Hz and the sweep time of 250 ms, as shown in the Figure 4 insert. Curves (i) and (ii) in the inset of Figure 4 are the SNL and the intensity noise of the LO, respectively. The intensity noise of the LO reached the SNL for analysis frequencies higher than 1.8 MHz.

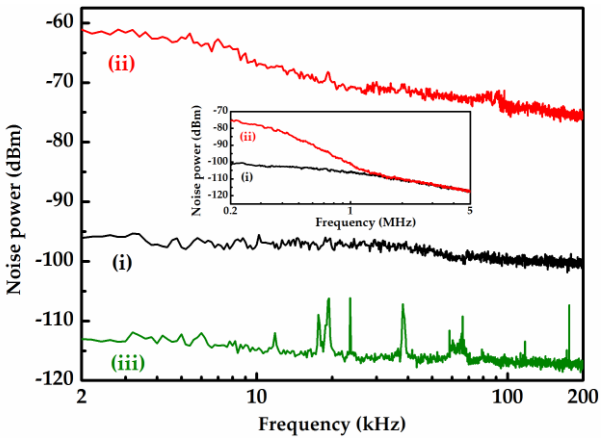

Figure 4. Intensity noise of the LO as a function of analysis frequencies: Curve (i), the SNL; Curve (ii), the intensity noise of the LO; and Curve (iii), the ENL. The inset is the intensity noise of the LO at analysis frequencies from 0.2 MHz to 5 MHz.

According to the theoretical calculation, when the intensity noise of the LO is 30 dB above the SNL at the analysis frequencies of 5 kHz, the value of CMRR of detectors should be higher than 54 dB to avoid the contamination of the squeezed light by intensity noise of the LO. For this purpose, the CMRR of photodetectors was measured firstly. The noise spectrum of the unbalanced detector, which was the common mode signal, was recorded by the SA when one photodiode was blocked and the other was illuminated at the power of 40 μW. The maximum allowed illuminated power was 50 μW, since the photodetector was easily saturated when photodetectors worked at unbalanced state with the self-subtraction photodetector scheme (one photodiode was blocked). However, when the squeezed vacuum states were measured, i.e., photodetectors worked at balanced state, the maximum allowed illuminated power was 5 mW. The illuminated laser was amplitude modulated using an EOM at different analysis frequencies. The noise spectrum of the balanced detector, that was the differential mode signal, was recorded when two photodiodes were illuminated at the power of 40 μW, respectively. The measured noise power from unbalanced detector and balanced detectors as a function of analysis frequencies is shown in Figure 5. The CMRR of photodetectors in the BHD system can be determined by the difference of noise power from balanced detectors and that from unbalanced detector. Dots were the measured data and curves were connected lines. It can be seen that the CMRR of photodetectors was higher than 60 dB at the range from 4 kHz to 20 kHz. The maximum CMRR of 67 dB was measured at the analysis frequency of 5 kHz. The CMRR was 54 dB at the analysis

frequency of 3 kHz. A typical example of the measurement for the CMRR of photodetectors at analysis frequency of 5 kHz is shown in the inset in Figure 5. Curves (i) and (ii) in the inset of Figure 5 are the photodetectors worked at unbalanced and balanced states, respectively. Curve (iii) in the inset of Figure 5 is the ENL. The CMRR was 67 dB at 5 kHz. Dots in Figure 5 were measured in this way at different audio-band analysis frequencies. The generated vacuum squeezed states could be effectively measured at audio-band frequencies with homemade high CMRR photodetectors.

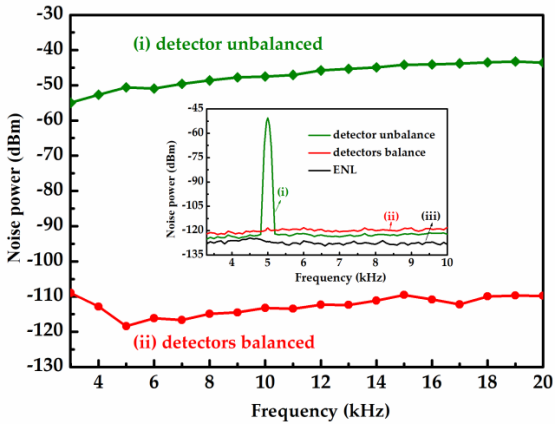

Figure 5. Measured noise power from unbalanced detector and balanced detectors as a function of analysis frequencies: Curve (i), detector unbalanced; and Curve (ii), detectors balanced. The CMRR of photodetectors in the BHD system was determined by the difference of noise power from balanced detectors and that from unbalanced detector. The inset is the measurement for the CMRR of photodetectors at the analysis frequency of 5 kHz.

In addition, the linearity of the BHD system was checked by measuring the SNL versus the total power of the LO, as shown in Figure 6. With the power of the LO doubly increasing, a clearance of 3 dB at analysis frequencies from 3.5 kHz to 20 kHz could be obtained from the total power of from 250 μW to 2 mW. The results show that the photodetector has linear response property in the given power range, and a larger clearance to mitigate the influence of dark noise. The total power of the LO of 1 mW was chosen for measuring the generated squeezed vacuum states because it could offer an electronic noise clearance of more than 20 dB at audio-band frequencies. In this case, the influence on measurement from the electronic noise could be ignored. Increasing the total power of the LO, it is possible that the extra noise of the LO would contaminate the observed squeezing level.

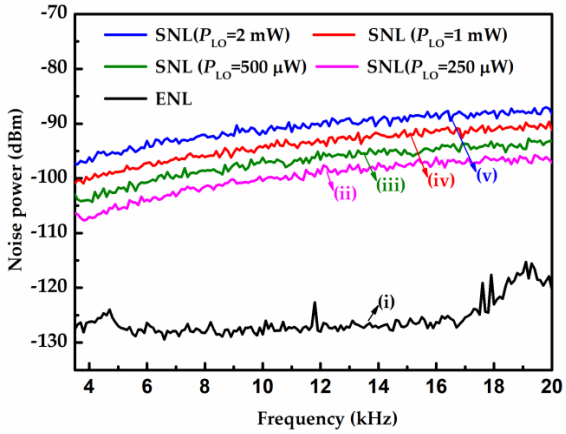

Figure 6. Linearity and clearance of photodetectors in the BHD system: Curve (i), the ENL; and Curves (ii)–(v), the SNL versus the total power of the LO (250 μW, 500 μW, 1 mW and 2 mW).

The measured threshold power of the OPO was 350 mW in the experiment. When the pump with the power of 100 mW and the CCF with the power of 100 μW were injected into the OPO, the OPO was operated below the threshold. The generated squeezed vacuum states were measured using the BHD system with the LO power of 1 mW and the fringe visibility of 99%. In the measurement of squeezed vacuum states at audio-band frequencies, the noise power traces also need to be averaged for some times to obtain the accurate result, thus requiring the experimental setups involved to be stable at the timescale of several tens of minutes [22]. When the relative phase between the squeezed vacuum states and LO was locked to $\pi/2$ and the relative phase between the pump and CCF was fixed to 0, the generated phase squeezed vacuum states could be measured stably. Figure 7 shows the measured noise power of phase squeezed vacuum states at analysis frequencies from 3.5 kHz to 20 kHz recorded by SA with an RBW of 50 Hz, a VBW of 100 Hz and the sweep time of 1 s. All noise power traces were averaged 20 times. Curves (i)–(iv) are the SNL, the squeezing noise, the anti-squeezing noise and the ENL, respectively. The measured squeezing degree of phase squeezed vacuum states at audio-band frequencies from 5 kHz to 20 kHz was approximately 6.1 ± 0.3 dB. The corresponding anti-squeezing was 10.1 ± 0.3 dB. A 3.0 ± 0.3 dB phase squeezed vacuum state was obtained at the audio frequency of 3.5 kHz. Considering the total detection losses of η_{esc} = 0.95, η_{det} = 0.96, η_{prop} = 0.94, and η_{hom} = 0.98, the theoretical calculated squeezing level is 6.25 dB, which is not dependent on the CMRR of the detectors. The theoretical prediction has a discrepancy with experimental results, a possible reason being that the anti-squeezed quadrature contaminates the measured squeezing level due to the phase jitter. Owing to the coherent locking scheme, the actual phase jitter was only about 1.7°, which was calculated according to the discrepancy between the theoretical prediction and experimental results. The measured squeezing level has a sharp reduction below around 4.5 kHz. The possible reason is squeezed variance spectra at these frequencies were contaminated by additional noise from scattered fields [23]. They were identified to originate from the micro-roughness of the optical surfaces, non-perfect anti-reflection coatings and residual transmissions of high reflection mirrors. The scattered light may be entering from the coherent locking setup or BHD setup.

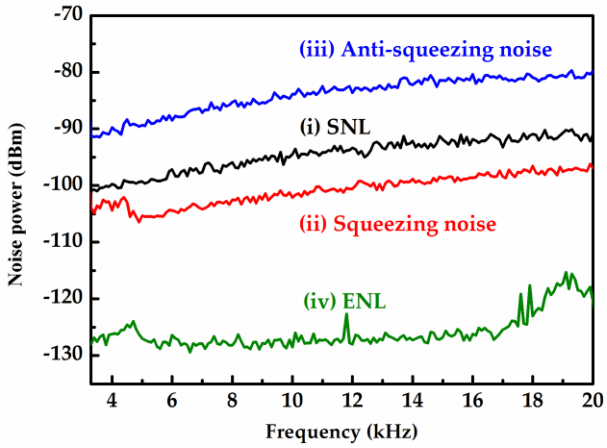

Figure 7. Measured noise power of the generated phase squeeze vacuum states at audio-band frequencies from 3.5 kHz to 20 kHz: Curves (i)–(iv), SNL, squeezing noise, anti-squeezing noise and ENL, respectively. The parameters of SA: RBW of 50 Hz, VBW of 100 Hz and sweep time of 1 s. All noise power traces were averaged 20 times.

Figure 8 shows the measured noise power of phase squeezed vacuum states at the audio frequency of 5 kHz recorded by SA with an RBW of 1 kHz and a VBW of 30 Hz, and the sweep time was 500 ms. All noise power traces were averaged 50 times. Curves (i)–(iii) are the SNL, the squeezing noise and the anti-squeezing noise, respectively. The generated phase squeezed vacuum state at the audio frequency of 5 kHz can be measured and recorded continuously.

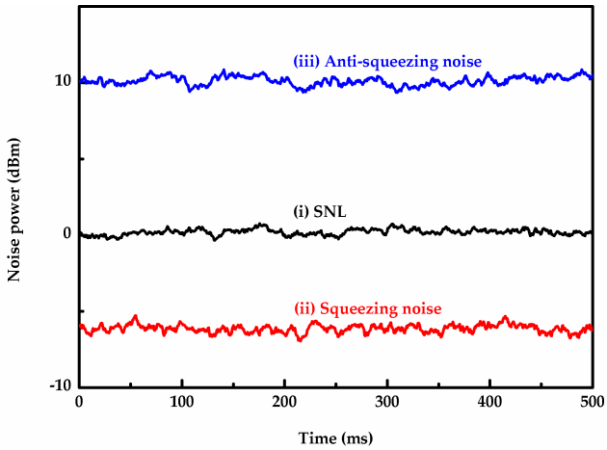

Figure 8. Measured noise power of the generated phase squeeze vacuum state at the audio frequency of 5 kHz: Curves (i)–(iii), the SNL, the squeezing noise and the anti-squeezing noise, respectively. The parameters of SA: RBW of 1 kHz, VBW of 30 Hz, and sweep time of 500 ms. All noise power traces were averaged 50 times.

5. Conclusions

We demonstrated the generation and measurement of the stable phase squeezed vacuum states at audio-band frequencies. A homemade cw single-frequency 532 nm and 1064 nm dual-wavelength laser was employed in the experiment. The OPO was pumped by 532 nm output of the laser and the threshold of the OPO was 350 mW. The 1064 nm output of the laser was used as the LO beam of the BHD system; the auxiliary beam to lock the length of the subthreshold OPO cavity; and the CCF beam to control the relative phase between the squeezed vacuum states and LO and the relative phase between the pump and CCF. When 532 nm pump power was 100 mW, the relative phase between the squeezed vacuum states and LO was locked to $\pi/2$ and the relative phase between the pump and CCF was fixed to 0, phase squeezed vacuum states were generated and recorded continuously. To detect vacuum squeezed states at audio-band frequencies, the effect of the LO noise, the CMRR of detectors and the phase jitter between the LO and squeezed vacuum field were considered. The power of the LO of the BHD system was optimized to 1 mW. The CMRR of photodetectors in the BHD was improved to be more than 60 dB at audio-band frequencies by employing the differential fine-tuning circuit and adjustable BV. The phase jitter between the LO and squeezed vacuum field was reduced to 1.7° with the help of the coherent locking scheme. Based on the above techniques, 6.1 $\pm$ 0.3 dB phase squeezed vacuum states at audio-band frequencies from 5 kHz to 20 kHz were generated, and a 3.0 $\pm$ 0.3 dB phase squeezed vacuum state was obtained at the audio frequency of 3.5 kHz.

Author Contributions: Conceptualization, Y.G., Y.L., J.F. and K.Z.; methodology, Y.G., J.F. and K.Z.; software, Y.L.; validation, Y.G. and Y.L.; formal analysis, J.F.; investigation, Y.G., Y.L. and J.F.; resources, Y.G., Y.L. and J.F.; data curation, J.F. and K.Z.; writing—original draft preparation, Y.G. and J.F.; writing—review and editing, J.F. and K.Z.; visualization, Y.L. and K.Z.; supervision, K.Z.; project administration, J.F. and K.Z.; and funding acquisition, K.Z.

Funding: This research was funded by National Key R&D Program of China (No. 2016YFA0301401), Fund for Shanxi "1331 Project" Key Subjects Construction (No. 1331KS).

Conflicts of Interest: The author declares no conflict of interest.

References

1. McKenzie, K.; Grosse, N.; Bowen, W.P.; Whitcomb, S.E.; Gray, M.B.; McClelland, D.E.; Lam, P.K. Squeezing in the audio gravitational-wave detection band. *Phys. Rev. Lett.* **2004**, *93*, 161105. [CrossRef]
2. Goda, K.; Miyakawa, O.; Mikhailov, E.E.; Saraf, S.; Adhikari, R.; Ckenzie, K.M.; Ward, R.; Vass, S.; Weinstein, A.J.; Mavalvala, N. A quantum-enhanced prototype gravitational-wave detector. *Nature Phys.* **2008**, *4*, 472–476. [CrossRef]

3. Haine, S.A.; Olsen, M.K.; Hope, J.J. Generating controllable atom-light entanglement with a raman atom laser system. *Phys. Rev. Lett.* **2006**, *96*, 133601. [CrossRef]
4. Akamatsu, D.; Akiba, K.; Kozuma, M. Electromagnetically induced transparency with squeezed vacuum. *Phys. Rev. Lett.* **2004**, *92*, 203602. [CrossRef] [PubMed]
5. Hsu, M.T.L.; Hétet, G.; Longdell, J.J.; Buchler, B.C.; Bachor, H.A.; Lam, P.K. Quantum study of information delay in electromagnetically induced transparency. *Phys. Rev. Lett.* **2006**, *97*, 183601. [CrossRef]
6. Horrom, T.; Singh, R.; Dowling, J.P.; Mikhailov, E.E. Quantum-enhanced magnetometer with low-frequency squeezing. *Phys. Rev. A* **2012**, *86*, 023803. [CrossRef]
7. Otterstrom, N.; Pooser, R.C.; Lawrie, B.J. Nonlinear optical magnetometry with accessible in situ optical squeezing. *Opt. Lett.* **2014**, *39*, 6533–6536. [CrossRef] [PubMed]
8. Taylor, M.A.; Janousek, J.; Daria, V.; Knittel, J.; Hage, B.; Bachor, H.A.; Bowen, W.P. Biological measurement beyond the quantum limit. *Nat. Photon.* **2013**, *7*, 229–233. [CrossRef]
9. Liu, C.J.; Jing, J.T.; Zhou, Z.F.; Pooser, R.C.; Hudelist, F.; Zhou, L.; Zhang, W.P. Realization of low frequency and controllable bandwidth squeezing based on a four-wave-mixing amplifier in rubidium vapor. *Opt. Lett.* **2011**, *36*, 2979. [CrossRef] [PubMed]
10. Vahlbruch, H.; Chelkowski, S.; Hage, B.; Franzen, A.; Danzmann, K.; Schnabel, R. Coherent control of vacuum squeezing in the gravitational-wave detection band. *Phys. Rev. Lett.* **2006**, *97*, 011101. [CrossRef]
11. McKenzie, K.; Gray, M.B.; Goßler, S.; Lam, P.K.; McClelland, D.E. Squeezed state generation for interferometric gravitational-wave detection. *Class. Quantum Gravity* **2006**, *23*, 245–250. [CrossRef]
12. Mehmet, M.; Ast, S.; Eberle, T.; Steinlechner, S.; Vahlbruch, H.; Schnabel, R. Squeezed light at 1550 nm with a quantum noise reduction of 12.3 dB. *Opt. Express* **2011**, *19*, 25763–25772. [CrossRef] [PubMed]
13. Stefszky, M.S.; Mow-Lowry, C.M.; Chua, S.S.Y.; Shaddock, D.A.; Buchler, B.C.; Vahlbruch, H.; Khalaidovski, A.; Schnabel, R.; Lam, Pa. K.; McClelland, D.E. Balanced homodyne detection of optical quantum states at audio-band frequencies and below. *Class. Quantum Gravity* **2012**, *29*, 145015. [CrossRef]
14. Breitenbach, G.; Schiller, S.; Mlynek, J. Measurement of the quantum states of squeezed light. *Nature* **1997**, *387*, 471–475. [CrossRef]
15. Kwee, P.; Willke, B.; Danzmann, K. New concepts and results in laser power stabilization. *Appl. Phys. B* **2011**, *102*, 515–522. [CrossRef]
16. Aoki, T.; Takahashi, G.; Furusawa, A. Squeezing at 946 nm with periodically poled KTiOPO4. *Opt. Express.* **2006**, *14*, 6930–6935. [CrossRef] [PubMed]
17. McKenzie, K.; Gray, M.B.; Lam, P.K.; McClelland, D.E. Technical limitations to homodyne detection at audio frequencies. *Appl. Opt.* **2007**, *46*, 3389–3395. [CrossRef] [PubMed]
18. Khalaidovski, A. Beyond the Quantum Limit: A Squeezed-Light Laser in GEO600. Ph.D. Thesis, University of Hannover, Hannover, Germany, November 2011; pp. 68–69.
19. Yang, W.H.; Jin, X.L.; Yu, X.D.; Zheng, Y.H.; Peng, K.C. Dependence of measured audio-band squeezing level on local oscillator intensity noise. *Opt. Express.* **2017**, *25*, 24262–24271. [CrossRef] [PubMed]
20. Hansen, H.; Aichele, T.; Hettich, C.; Lodahl, P.; Lvovsky, A.I.; Mlynek, J.; Schiller, S. An ultra-sensitive pulsed balanced homodyne detector: Application to time-domain quantum measurement. *Opt. Lett.* **2001**, *26*, 1714–1716. [CrossRef]
21. Drever, R.W.P.; Hall, J.L.; Kowalski, F.V.; Hough, J.; Ford, G.M.; Munley, A.J.; Ward, H. Laser phase and frequency stabilization using an optical resonator. *Appl. Phys. B* **1983**, *31*, 97–105. [CrossRef]
22. Khalaidovski, A.; Vahlbruch, H.; Lastzka, N.; Gräf, C.; Danzmann, K.; Grote, H.; Schnabel, R. Long-term stable squeezed vacuum state of light for gravitational wave detectors. *Class. Quantum Gravity* **2012**, *29*, 075001. [CrossRef]
23. Vahlbruch, H.; Chelkowski, S.; Danzmann, K.; Schnabel, R. Quantum engineering of squeezed states for quantum communication and metrology. *New J. Phys.* **2007**, *9*, 371. [CrossRef]